Available online at www.sciencedirect.com
SCIENCE DIRECT®
Journal of Molecular Catalysis A: Chemical 208 (2004) 147–158
JOURNAL OF MOLECULAR CATALYSIS A: CHEMICAL
www.elsevier.com/locate/molcata

Effect of a Lewis acid additive on active sites formation in zirconocene catalyst systems: a DFT study

P.G. Belelli [a], D.E. Damiani [b], N.J. Castellani [a,*]

[a] *Departamento de Física, Universidad Nacional del Sur (UNS), Avenida Alem 1253, 8000 Bahía Blanca, Argentina*
[b] *Planta Piloto de Ingeniería Química, PLAPIQUI (UNS-CONICET), Camino La Carrindanga Km 7, 8000 Bahía Blanca, Argentina*

Received 4 August 2003; received in revised form 4 August 2003; accepted 5 August 2003

Abstract

Comparative theoretical analysis of optimized geometries and electronic structures of Cp_2ZrCl_2/methylaluminoxane (MAO) system and its interactions with a third component was performed. The additive studied was a Lewis acid compound: $AlCl_3$. Density functional theory (DFT), that included exchange and correlation effects, was employed with Gaussian basis sets. Additive enhances the cocatalyst Lewis acid character and, indirectly, it modifies the electrophilicity of Zr atom. By comparing the geometrical structure and charge distribution of the site with and without $AlCl_3$ it is possible to understand the reasons of polymerization performance improvement. Previous experimental results for these systems have showed a notable increase in ethylene and propylene polymerization activity.

Keywords: Metallocenic system; DFT studies; $AlCl_3$ addition

1. Introduction

The chemical industry of polyolefins where millions of tons of polyethylene are produced per year constitutes one of the biggest consumers of catalysts, with its natural economic implications. Moreover, the appearance of a new generation of catalysts able to yield polymers with well defined structure and physical properties increase the importance of research efforts in the field of polymerization catalysts. The novel technologies are based on transition metal complexes, such as the metallocenes combined with a cocatalyst as methylaluminoxane (MAO), providing a high active and selective catalyst, even more than the traditional Ziegler-Natta catalysts [1]. The study of these systems undergoes a daily actualization. At the experimental level, ^{1}H NMR, ^{13}C NMR, FTIR, UV-Vis and Raman spectroscopies have been employed for the chemical characterization and to study its relationship with the polymerization capability [2]. Despite the amount of work made to elucidate the nature and reactive properties of active sites, there are still open several questions.

Very recently, an experimental work has shown interesting changes of usual catalytic activity of *rac*-$EtInd_2ZrCl_2$/MAO used to polymerize ethylene and propylene under standard reacting conditions [3]. Results show that the addition of $AlCl_3$ produces an increase of nearly 50 and 25% in polyethylene and propylene yields, respectively. A subsequent study using UV-Vis spectroscopy allowed to associate these catalytic activity changes with an electronic effect of $AlCl_3$ on the cation-like metallocenium. The absorption intensity changes of typical "ligand to metal charge transfer" band (LMCT) could be explained as an electronic density modification of Zr atom in the cation species.

Regarding these results, a study based on theoretical methods was considered very interesting as a complementary approach to the problem. The noticeably advances achieved last years in computational facilities allows the implementation of theoretical calculations for large and complex chemical systems. Furthermore, the widely reliability of first principle codes including exchange and correlation effects has been possible with the use of density function theory (DFT) [4]. These calculation methods provide us valuable quantitative and qualitative information,

* Corresponding author. Tel.: +54-291-4595141; fax: +54-291-4595142.
E-mail addresses: pbelelli@criba.edu.ar (P.G. Belelli), castella@criba.edu.ar (N.J. Castellani).

1381-1169/$ – see front matter © 2003 Elsevier B.V. All rights reserved.
doi:10.1016/j.molcata.2003.08.001

which can be contrasted with experiments. Therefore, the application of theory has a double significance, it can be used as a prediction tool or as a way to rationalize the analysis of experimental results. Anyway, theoretical models are proposed according to some experimental data or conditions, making from an interactive experimental–theoretical methodology an original way of research working.

In order to obtain a deeper understanding of previously commented experimental results, we studied what changes in geometry of active sites of Cp_2ZrCl_2/MAO system are produced as a consequence of addition of $AlCl_3$. We are also interested in the inherent electronic structure modifications undergone by our system model. In particular, the formation reaction energies of active sites and the relevant electronic population parameters were evaluated. We believe that the observations and consequences obtained in the present work will also provide by analogy useful information for other more complex metallocenic systems.

2. Computational details

Geometry optimization for our molecular model of catalytic site and each of its fragments were performed within the DFT formalism, using the hybrid functional which mixes the Lee, Yang and Parr functional for the correlation part and Becke's three-parameter functional for exchange (B3LYP) [5]. Molecular orbitals were expanded with a gaussian basis set, namely the split valence 3-21G** basis, including polarization p-type functions on hydrogen atoms and d-type functions on C, O, Al and Cl atoms. On the Zr atom, the 3-21G basis was used for valence orbitals and the Los Alamos Effective Core Potential plus Double Z (LANL2DZ) basis set for inner orbitals. This last basis set uses an effective core potential for the Zr core electrons, taking into account some relativistic effects for transition elements. All calculations reported in this work were carried out with the Gaussian'98 package of programs [6].

The following reactions where $AlCl_3$ is present have been considered for an energetic analysis:

$$Cp_2ZrCl_2 + 2MAO\text{-}CH_3{}^*AlCl_3 \rightarrow \text{active site (ionic-pair)} + MAO\text{-}Cl^*AlCl_3 \quad (1)$$

$$Cp_2ZrCl_2 + 2MAO\text{-}CH_3{}^*AlCl_3 \rightarrow Cp_2ZrCH_3{}^+ + MAO\text{-}CH_3Cl^{-*}AlCl_3 + MAO\text{-}Cl^*AlCl_3 \quad (2)$$

$$Cp_2ZrCH_3{}^+ + MAO\text{-}CH_3Cl^{-*}AlCl_3 \rightarrow \text{active site (ionic-pair)} \quad (3)$$

where active site (ionic-pair) represents the species $Cp_2ZrCH_3{}^+ \cdots MAO\text{-}CH_3Cl^{-*}AlCl_3$.

Eq. (1) differs from Eq. (2) in the kind of involved active site. The first of them implies the formation of an ionic-pair like active site while in the second case the active catalytic species is constituted by a cation and an anion isolated as it was supposed in several previous models [7]. Eq. (3) is reserved for the formation of an ionic-pair like active site directly from the ionic fragments. The reaction energies corresponding to both reactions (1) and (3) have been computed for two kinds of ionic-pairs. Each one of them depends on the way the zirconocene approaches the cocatalyst approach. Then the influence of additive was taken into account. The balance of total energy ΔE for Eqs. (1)–(3) gives the following expressions:

$$\Delta E = E_T(\text{ionic-pair}) + E_T(MAO\text{-}Cl^*AlCl_3) - E_T(Cp_2ZrCl_2) - 2E_T(MAO\text{-}CH_3{}^*AlCl_3) \quad (1.E)$$

$$\Delta E = E_T(Cp_2ZrCH_3{}^+) + E_T(MAO\text{-}CH_3Cl^{-*}AlCl_3) + E_T(MAO\text{-}Cl^*AlCl_3) - E_T(Cp_2ZrCl_2) - 2E_T(MAO\text{-}CH_3{}^*AlCl_3) \quad (2.E)$$

$$\Delta E = E_T(\text{ionic-pair}) - E_T(Cp_2ZrCH_3{}^+) - E_T(MAO\text{-}CH_3Cl^{-*}AlCl_3) \quad (3.E)$$

The full counterpoise procedure was applied to correct the basis set superposition error (BSSE) [8]. Due to the fact that this method is particularly suitable when the reactants do not undergo important modifications of their geometries after bond formation, this correction was applied only in some cases as it will be shown below.

The net atomic and molecular charges were obtained with the natural bond orbital (NBO) analysis [9]. A study of certain orbital overlap populations was also performed according to Mülliken's technique [10]. The charge density difference $\Delta\rho(r)$ and the Laplacian $\nabla^2\rho(r)$ were plotted for the optimized geometries of active sites in order to have a two-dimensional representation of the electronic structure changes of ionic-pairs due to the presence of additive. The $\Delta\rho(r)$ plot was obtained computing the difference of the electron density point to point between the ion pair and the isolated cation complex plus the isolated $MAO\text{-}CH_3Cl^{-*}AlCl_3$ counterion (i.e. counterion modified with $AlCl_3$ additive). To accomplish these analyzes it was essential to use the same geometries for the ion pair and the isolated species.

3. Models

3.1. Model of cocatalyst: MAO

The molecular models used here for the MAO-CH_3 cocatalyst and the $MAOCH_3Cl^-$ counterion were studied in a previous work, where a more detailed explanation of its fundamentals can be found [11]. Basically, these models have been proposed taking into consideration the more recent MAO models, in which "cage-like" structures are used

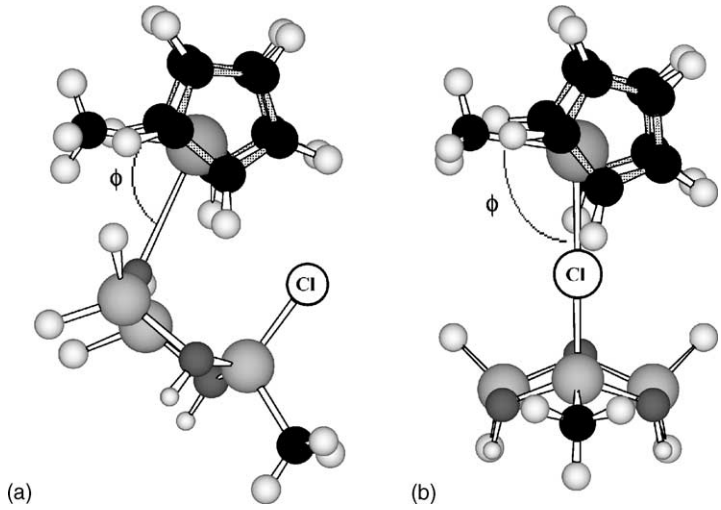

Fig. 1. Optimized geometry of (a) Site 1; (b) Site 2.

[12]. The main reason for explaining the existence of large MAO aggregates is the greater stability of tetra-coordinated Al atoms compared with the tri-coordinated ones, yielding dative covalent bonds O → Al [13]. Our MAO-CH_3 model has alternated Al and O atoms in the corners of two rings with four-members each one. The MAO-CH_3Cl^- model, where the MAO acts as counterion, has a chlorine ion taken from the zirconocene. This MAO ability to extract a X^- ion from a metallocene is due to the latent acidity of two rings of MAO.

The effect of cluster size for both MAO-CH_3 and MAO-CH_3Cl^- counterion has been evaluated [11], concluding that the information related to the energy formation of active sites attained with the smaller models was of sufficient accuracy. By this reason our study of electronic structure changes was performed on the more reduced MAO clusters in which only the most near interaction region to the cation-like metallocenium has been included.

3.2. Zirconocene and ion pair formation

The models above commented for the $Cp_2ZrCH_3^+$ cation and the MAO-CH_3Cl^- counterion allow us to define two different active catalytic sites, which were described and analyzed in a the commented previous work [11]. These cation-counterion species constitute ionic-pairs of high stability. They can be differentiated by the geometrical configuration and the degree of contact between the partners of the site [2b,14]. In Site 1 the nearest interaction of Zr is with the central O atom of counterion (see Fig. 1a). On the other hand, in Site 2 the interaction is established through a chlorine bridge (see Fig. 1b). In this theoretical study the modifications undergone by both sites due to the presence of $AlCl_3$ additive have been considered.

4. Results and discussion

As it was mentioned in Section 1, in a previous experimental work a metallocene-like system with the addition of $AlCl_3$ was evaluated as a catalyst in homogeneous phase for the polymerization of ethylene and propylene [3]. The results indicated a significant increase of activity towards the production of simple polymers. From the analysis of UV-Vis spectra for the cocatalyst/$AlCl_3$ and zirconocene/cocatalyst/$AlCl_3$ systems it was concluded that these three components interact between them. Indeed, the additive changes the electrophilicity of Zr atoms acting in an indirect way through the cocatalyst [14c]. A small decrease of electronic charge of Zr could be one of the reasons for the higher activity in this modified homogeneous catalyst. We desire to verify this trend and to attain a deeper understanding of this property in terms of quantum mechanical arguments. Then, a careful study of geometrical changes of active sites and the analysis of atomic charges, interatomic overlap populations and charge transfers were performed. Moreover, the reaction energies defined in Section 2 for the main chemical processes were also included as an element of discussion.

4.1. MAO*$AlCl_3$ models

Before considering the active site plus additive as an entire entity, the chemical reaction between cocatalyst and additive was first studied. The justification for this procedure was that in the experiments MAO and $AlCl_3$ were introduced in the reactor before zirconocene in order to achieve a close interaction between them. Comparing the UV-Vis spectra of MAO and the product produced within the reactor we confirmed that these compounds interact strongly assuring that a new species has been formed. It can be named the modified cocatalyst MAO*$AlCl_3$.

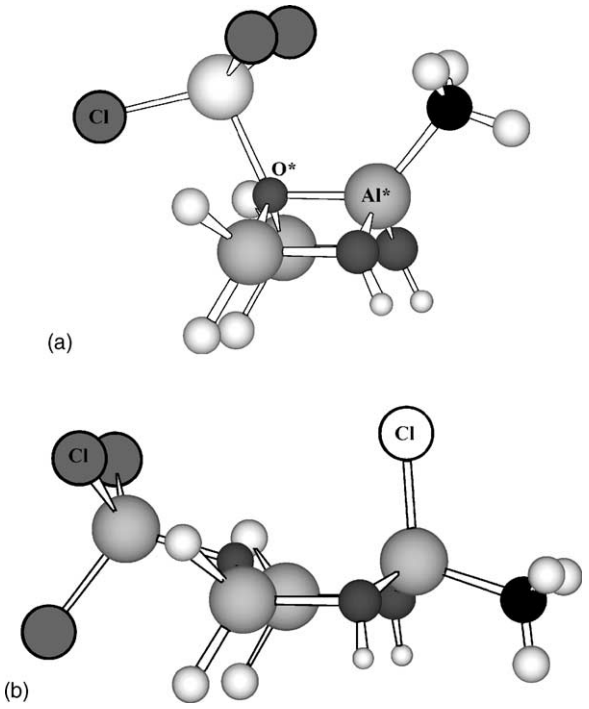

Fig. 2. (a) Lateral view of MAO-CH_3*$AlCl_3$ model. (b) Lateral view of MAO-CH_3Cl^-*$AlCl_3$ counterion model.

The study of the interaction of $AlCl_3$ and the model for MAO (see Section 3.1) comprised the full optimization of atomic coordinates, fixing only certain internal MAO angles, as it was part of a greater tridimensional cage-like structure. In Fig. 2a and b the final species of MAO-CH_3*$AlCl_3$ cocatalyst and MAO-CH_3Cl^-*$AlCl_3$ counterion are pictured, respectively. In both cases the lowest total energy was attained for the Al atom of additive linked with the central oxygen atom O* of MAO. The corresponding optimized Al_{AlCl3}–O* distances for $AlCl_3$ interacting with MAO-CH_3 and MAO-CH_3Cl^- are of 1.985 and 1.926 Å, respectively. These distances are only ∼0.15 Å greater than the internal Al–O distances of non-modified MAO counterparts. This significant shortening of Al_{AlCl_3}-O* distance for the counterion is related to the modifications undergone by the MAO structure. Indeed, the opening of dative central O* → Al* bond diminishes the internal stress of four-member ring and, then, the steric hindrance due to the methyl group linked with the aluminium atom Al* of MAO is alleviated. Another local energy minimum has been found when $AlCl_3$ binds with one of lateral O atoms of MAO. In this case, the Al_{AlCl_3}–O distance is greater (2.139 Å) and the energy higher (E_T shift = 20 kcal/mol).

In Table 1 the NBO atomic and molecular charges for the most important atoms of the MAO species, MAO-CH_3 and MAO-CH_3Cl^- and its respective $AlCl_3$-modified species, are summarized. Atomic charges of MAO-CH_3*$AlCl_3$ and MAO-CH_3Cl^-*$AlCl_3$ are, compared with their counterparts without additive MAO-CH_3 and MAO-CH_3Cl^-, slightly modified. The positive charge of central aluminiun atom Al* is always higher than those of remaining aluminium atoms of the model indicating its higher Lewis acid character. This charge increases due to the presence of additive, hence, an acidity enhancement of Al* can be predicted when MAO is in contact with $AlCl_3$.

Making a general analysis of atomic charges, we infer that the additive modifies the charge distribution inside each evaluated species. Indeed, a negative charge abstraction mediated by the $AlCl_3$ additive can be observed in the MAO-CH_3 cocatalyst as well as in the MAO-CH_3Cl^- counterion. The MAO species without $AlCl_3$ gain positive charge, being this effect the most evident for the counterion fragment (0.0 versus 0.12e and −1.00 versus −0.76e for cocatalyst and counterion, respectively). Once more, we notice that the increase of Lewis acid character in the analyzed species is verified by the predicted charge values.

From the same table we observe that the central dative bond O* → Al* for MAO-CH_3 is more polarized in presence of $AlCl_3$ additive, giving a more labile bond. This observation is consistent with the Mülliken overlap population (OP) results exhibited in Table 2. The OP value of this bond decreases substantially (by ∼60%). The other internal O*–Al bonds decrease in a lower degree (by ∼35–38%). A similar result can be noticed when the additive is added to MAO-CH_3Cl^- counterion. However, in this case the O* → Al* bond continues being broken. A non-negligible positive OP value is obtained for the O*–Al_{AlCl_3} bond, indicating that a O*–Al_{AlCl_3} bond is formed when the $AlCl_3$ is coordinated

Table 1
NBO charge analysis for the principal atoms of MAO-CH_3*$AlCl_3$ and MAO-CH_3Cl^-*$AlCl_3$ counterion

Atoms and species	MAO-CH_3 (a.u.)	MAO-CH_3Cl^- (a.u.)	MAO-CH_3*$AlCl_3$ (a.u.)	MAO-CH_3Cl^-*$AlCl_3$ (a.u.)
MAO-CH_3	0.00	−1.00	0.12	−0.76
$AlCl_3$	–	–	−0.12	−0.24
Al*	1.73	1.63	1.76	1.67
Al	1.23	1.15	1.17	1.18
Al	1.23	1.15	1.17	1.20
O*	−1.13	−1.07	−1.19	−1.20
Cl	–	−0.56	–	−0.54
Al_{AlCl_3}	–	–	1.38	1.50
Cl_{AlCl_3}	–	–	−0.50	−0.58

$AlCl_3$ is bonded with O* atom. MAO-CH_3 and MAO-CH_3Cl^- are included for comparison.

Table 2
Overlap population parameter corresponding to MAO-CH_3, MAO-CH_3Cl^- species and the $AlCl_3$ counterpart

Dative bond	MAO-CH_3	MAO-CH_3Cl^-	MAO-$CH_3{}^*AlCl_3$	MAO-$CH_3Cl^{-*}AlCl_3$
$O^* \rightarrow Al^*$	0.384	0.072	0.154	0.066
$O^* \rightarrow Al_1$	0.476	0.672	0.314	0.436
$O^* \rightarrow Al_2$	0.486	0.676	0.298	0.432
$O^* \rightarrow Al_{AlCl_3}$	–	–	0.238	0.494

around the central O^* atom of the cocatalyst model. In the cases of the counterion species this bond shows a higher OP value, which can be related to the scission of the central $O^* \rightarrow Al^*$ bond. In consequence, from our results we can infer that the Lewis acid character of MAO-$CH_3{}^*AlCl_3$ cocatalyst and MAO-$CH_3Cl^{-*}AlCl_3$ counterion increases due to the interactions with the $AlCl_3$ additive.

It is generally accepted that the cocatalyst acts in different ways during the active sites formation and that its Lewis acid property is essential for this purpose [15]. In case of a dichloride zirconocene the alkylation is the first step in the metallocene–cocatalyst interaction. For this reason, the alkylation reaction was used as a test reaction for the Lewis acid strength of our modified cocatalyst model, MAO-$CH_3{}^*AlCl_3$, in comparison with the MAO-CH_3 cocatalyst model:

$$Cp_2ZrCl_2 + \text{MAO-}CH_3{}^*AlCl_3 \rightarrow Cp_2ZrClCH_3 + \text{MAO-Cl}^*AlCl_3 (\text{and without } AlCl_3)$$

The corresponding energy balance values of this reaction indicate that the dichloride zirconocene alkylation is thermodynamically favored in presence of $AlCl_3$-modified cocatalyst (-107.91 kcal/mol versus -66.95 kcal/mol, with respect to the non-modified cocatalyst). These results are in agreement with the expected increase of Lewis acid strength of cocatalyst, as it was previously concluded from NBO atomic charge and Mülliken overlap population. Experimental observations of ethylene and propylene polymerization can be related with these theoretical results [3]. Kinetic curves for *rac*-$EtInd_2ZrCl_2$/MAO$^*AlCl_3$, when compared with the same system without additive, showed an increase of olefin consumption in the initial period of reaction.

4.2. Active sites models

4.2.1. Optimized parameters

The molecular structure of active sites designed as Site 1 and Site 2 were also optimized in presence of $AlCl_3$, obtaining two stable geometries for the zirconocene plus $AlCl_3$-modified counterion system. The final geometrical position of additive in the MAO model depends on the active sites analyzed. For Site 1 the $AlCl_3$ was coordinated to a lateral oxygen atom (Fig. 3). In case of Site 2 the additive was linked with the central oxygen atom O^* (Fig. 4). The most relevant distances and angle bonds for both active species formed with MAO-$CH_3Cl^{-*}AlCl_3$ counterion are summarized in Table 3. The same parameters corresponding to the sites with non-modified counterion were also included for comparative purposes. The overall geometry of Site 1 shows no significant changes. The most important modifications are noticed on the $Zr–C_{CH_3}$ and $Zr–O^*$ distances. The additive produces a $Zr–C_{CH_3}$ bond elongation that is in agreement with other reports [16]. The variation of this bond length is analogous to that observed when an olefin

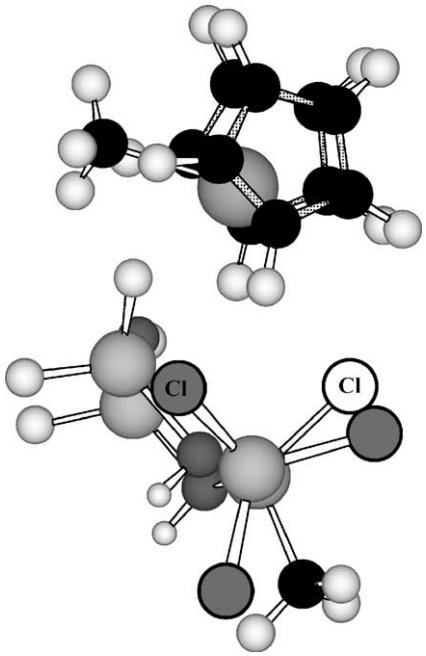

Fig. 3. Optimized geometry of Site 1 with MAO-$CH_3Cl^{-*}AlCl_3$.

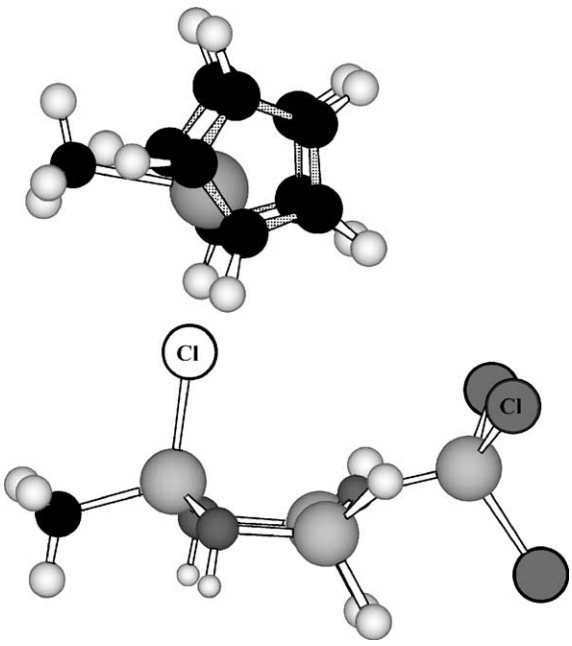

Fig. 4. Optimized geometry of Site 2 with MAO-$CH_3Cl^{-*}AlCl_3$.

Table 3
Optimized distance and angle bonds obtained from $Cp_2ZrCH_3^+ \cdots MAO\text{-}CH_3Cl^{-*}AlCl_3$ for both type of sites

Parameter	Optimized parameter[a]			
	Site 1	Site 2	Site 1*$AlCl_3$	Site 2*$AlCl_3$
Zr–Cl distance	3.738	2.580	3.801	2.685
Zr–O* distance	2.946	5.491	2.970	5.566
Zr–C_{Me} distance	2.269	2.264	2.304	2.296
Al*–Cl distance	2.116	2.194	2.116	2.179
ϕ Angle (Fig. 1)	73.7	102.2	74.5	93.3
α Diedral angle	10.0	135.1	7.8	218.9
Al_{AlCl_3}-OMAO	–	–	2.127	1.926
Al–Cl ($AlCl_3$)	–	–	2.095	2.155

Parameters of active sites without $AlCl_3$ are included.
[a] Distances expressed in Å and bond angles in °.

molecule, like ethylene, is coordinated to Zr atom in the initial step or in the transition state of olefin insertion. In addition, a slightly increase of the ϕ angle indicates a more open gap of the active site. On the other hand, the dihedral angle α that measures the rotation of the $MAO\text{-}CH_3Cl^{-*}AlCl_3$ counterion with respect to the cation, undergoes a very small change. The interaction between Zr and Cl atoms could be responsible of the negligible modification of this angle.

In case of the Site 2, the Zr–Cl bond becomes more elongated, this effect being accompanied with a Al*–Cl bond shortening. These changes produce a looseness of ions in the ionic-pair due to the contingent Zr–Al* distance increases (4.774 Å for Site 2 versus 4.863 Å for Site 2 with $AlCl_3$). As it was mentioned for Site 1, the Zr–C_{CH_3} bond is also elongated. Nevertheless, this effect is more important for Site 1 than for Site 2. Besides, the overall geometrical structure is noticeably modified with respect to the active site without additive. Indeed, the dihedral angle α shows a 60% increase, giving a more symmetrical site (see Table 3). This notable variation of the α angle occurs through the chlorine bridge between the Al* atom of counterion and Zr atom of cation. Taking into account these results it is possible to infer that the $AlCl_3$ additive favors a more open active site with a stretching of Zr–C_{CH_3} bond. These new characteristics could be the responsible to achieve enhancement productivity in olefin polymerizations [3].

Table 5
Mülliken overlap population parameter corresponding to Cp_2ZrCl_2, Site 1, Site 2, Site 1*$AlCl_3$ and Site 2*$AlCl_3$ species

Species	Zr–C_{Me}	Zr–Cl	Zr–O*	Al*–Cl
Cp_2ZrCl_2	–	0.454	–	–
Site 1	0.472	0.036	0.252	0.452
Site 2	0.520	0.188	−0.004	0.222
Site 1*$AlCl_3$	0.484	0.03	0.232	0.474
Site 2*$AlCl_3$	0.536	0.15	−0.004	0.298

4.2.2. Charges and overlap analysis

In Table 4 the NBO charges for the active sites with and without additive are summarized. Taking into account the net molecular charges of two ionic components of the ionic-pair, the $AlCl_3$ induces a more polarized ionic-pair. The negative loss from zircocation is evidenced in the electron deficiency of Zr atom. Furthermore, a redistribution of charges is produced in Site 2 between the Cp ligands and the methyl group of cation. In particular the electrons distribute more symmetrically in both π-ligands. This result can be explained because the Cp rings are placed more symmetrically with respect the $MAO\text{-}CH_3Cl^{-*}AlCl_3$ counterion. Notice in Fig. 4 the presence of a mirror plane as a consequence of the large value of the dihedral angle α.

In addition, the atomic charges of Zr and C (of methyl group) atoms present a higher difference with respect to the active sites without additive, suggesting that the Zr–C_{CH_3} bond has a weak covalent character. On the other hand, the negative molecular charge of $AlCl_3$ is higher in magnitude in Site 2 than in Site 1. Hence, the electron withdraw effect produced by the additive on the ionic-pair is more pronounced if the $AlCl_3$ is coordinated with the central O* atom.

From the OPs presented in Table 5 it is possible to analyze the cation–anion interaction. In all the cases the orbital overlap of Zr–Cl bonds are very low. However, higher

Table 4
NBO charge analysis of $Cp_2ZrCH_3^+ \cdots MAO\text{-}CH_3Cl^-$ and $Cp_2ZrCH_3^+ \cdots MAO\text{-}CH_3Cl^{-*}AlCl_3$ for both types of sites

Atoms and species	$MAO\text{-}CH_3Cl^-$	$MAO\text{-}CH_3Cl^{-*}AlCl_3$	$Cp_2ZrCH_3^+$	Site 1	Site 2	Site 1*$AlCl_3$	Site 2*$AlCl_3$
$Cp_2ZrCH_3^+$	–	–	1	0.81	0.77	0.84	0.82
Zr	–	–	1.84	1.79	1.71	1.81	1.74
Cp_1	–	–	−0.23	−0.30	−0.31	−0.30	−0.26
Cp_2	–	–	−0.23	−0.31	−0.24	−0.31	−0.26
C_{CH_3}	–	–	−1.11	−1.05	−1.09	−1.06	−1.10
$MAO\text{-}CH_3Cl^-$	−1.00	−1.00 (with $AlCl_3$)	–	−0.81	−0.77	−0.84 (with $AlCl_3$)	−0.82 (with $AlCl_3$)
Cl	−0.56	−0.54	–	−0.56	−0.50	−0.54	−0.52
O*	−1.07	−1.20	–	−1.11	−1.08	−1.10	−1.20
Al*	1.63	1.67	–	1.67	1.72	1.67	1.74
$AlCl_3$	–	−0.24	–	–	–	−0.10	−0.23
Al_{AlCl_3}	–	1.50	–	–	–	1.43	1.48
Cl_{AlCl_3}	–	−0.58	–	–	–	−0.51	−0.57

The comparison was accomplished taking into account the Cp_2ZrCl_2 catalyst and the isolated cation and $MAO\text{-}CH_3Cl^-$ counterion. Charges expressed in a.u.

values had been obtained for Site 2, likely because in this case the zirconocene–cocatalyst interaction is realized only through the Cl atom. The calculated OP of Zr–O* bond in Site 1 has a much higher value than the Zr–Cl bond in Site 2, indicating that a stronger cation–anion interaction occurs in Site 1. On the other hand, the OP values of Zr–O* bond in Site 2 corresponds to a non-bonding interaction. Notice that the OP values of Zr–O* bond in Site 1 and Zr–Cl bond in Site 2 are reduced when the counterion interacts with additive. This weakening of cation–anion interaction is greater for Site 2 than for Site 1 (20% versus 8% reductions of commented OPs, respectively). Thus, for both cases the results indicate a loosened ionic-pair formation favoring the posterior coordination of a monomer molecule. With respect to the OP of Zr–C_{CH_3} bonds, they become slightly increased (∼3%), whilst the Zr–C_{CH_3} distances increase also slightly. The reason of this distance stretching cannot be related in this case simply to the OP changes.

4.2.3. Reaction energies analysis

In Table 6 the calculated values for active sites formation with and without $AlCl_3$ are summarized. The reactions were evaluated using the Eqs. (1)–(3) presented in Computational Details Section. The results of Eq. (1) clearly indicate that the active site formation with the addition of $AlCl_3$ is thermodynamically favored. The polymerization reactions with [$AlCl_3$]:[Zr] molar ratios of 1 or higher are highly affected with an increase of 60 and 100% in the reaction energy for Site 1 and for Site 2, respectively. From the data presented in Table 6 is also possible to observe the relative stability of the active sites in presence of additive. The active Site 1 is 9.13 kcal/mol more unstable than Site 2. The different position where $AlCl_3$ links with the counterion could be related to this behavior. The $AlCl_3$ coordination in the MAO-CH_3Cl^- counterion results to be thermodynamically more favored on the central O* atom than on the lateral oxygen atom, as it was presented in Section 4.1. Therefore, the second possibility is likely less convenient than the additive bonded to the central O* atom. Besides, as the Site 1 is sterically more hindered by the coordinated additive and the ability of counterion for interacting with zircocation is affected due to the constrained geometry. On the other hand, the Site 2 modified with $AlCl_3$ has a higher distance between cation and anion, making a more open and less geometrically constrained site. This situation decreases the possibility of a repulsive interaction of steric origin between zircocation and additive.

Additional studies with a MAO cluster of higher size were performed. The aim of these calculations was to evaluate the behavior of these active sites without the steric hindrance introduces by $AlCl_3$. The MAO cage, designed here as cage_MAO structure, was modeled taking into account the considerations outlined in a previous work [11]. The $AlCl_3$ additive was linked with the central O atom in the external shell of cage_MAO. Hence, the additive position was the same for both active sites. The distances and angle bonds obtained after optimization of active sites with cage_MAO-$CH_3Cl^{*-}AlCl_3$ counterion do not experience notable differences with respect to the results for active sites with the smaller model of $AlCl_3$-modified counterion. From this analysis we deduce that the formation of Site 1 is now 28.13 kcal/mol more exothermic than the Site 2. In other words, the elimination of the steric hindrance in Site 1 makes this site more favored than the other one.

From the ΔE results for both active sites, it is possible to measure the energy destabilization due to $AlCl_3$. Looking the ΔE changes at the last column in Table 6, for the smaller MAO-$CH_3Cl^{-*}AlCl_3$ counterion, we observe that the Site 1 destabilizes 28.86 kcal/mol due to action of $AlCl_3$ in comparison with Site 2. On the other hand an energy stabilization of the same magnitude is obtained for Site 1 using the cage_MAO-$CH_3Cl^{-*}AlCl_3$ counterion, independently of a steric hindrance influence. Under the assumption that the additive affects in same way the formation of both active species we could infer that, at mean, the steric energy destabilization of Site 1 produced by the additive has a value of ∼30 kcal/mol. Therefore, the destabilization is eliminated when the $AlCl_3$ coordinates away from the interaction zone. In absence of steric hindrance the relative stabilization of the active sites does not change.

Table 6
Predicted reaction energies of $Cp_2ZrCH_3^+\cdots$MAO-CH_3Cl^- and $Cp_2ZrCH_3^+\cdots$MAO-$CH_3Cl^{-*}AlCl_3$ for both types of sites

Equation number	Reaction	ΔE with $AlCl_3$[a]	ΔE without $AlCl_3$[a]	ΔE change[a]
1	$Cp_2ZrCl_2 + 2MAO\text{-}CH_3^*AlCl_3 \rightarrow Cp_2ZrCH_3^+\cdots(\mu_1O^*)MAO\text{-}CH_3Cl^{-*}AlCl_3$ (Site 1) + MAO-Cl^*AlCl_3	−202.28	−126.18	−76.10
1	$Cp_2ZrCl_2 + 2MAO\text{-}CH_3^*AlCl_3 \rightarrow Cp_2ZrCH_3^+\cdots(\mu_1Cl)MAO\text{-}CH_3Cl^{-*}AlCl_3$ (Site 2) + MAO-Cl^*AlCl_3	−211.41	−106.45	−104.96
2	$Cp_2ZrCl_2 + 2MAO\text{-}CH_3^*AlCl_3 \rightarrow Cp_2ZrCH_3^+ + MAO\text{-}CH_3Cl^{-*}AlCl_3 + MAO\text{-}Cl^*AlCl_3$	−125.45	−11.39	−114.06
3	$Cp_2ZrCH_3^+ + MAO\text{-}CH_3Cl^{-*}AlCl_3 \rightarrow Cp_2ZrCH_3^+CH_3^+\cdots(\mu_1O^*)MAO\text{-}CH_3Cl^{-*}AlCl_3$ (Site 1)	−76.44 (−76.83)[b]	−114.80 (−114.93)[b]	38.36
3	$Cp_2ZrCH_3^+ + MAO\text{-}CH_3Cl^{-*}AlCl_3 \rightarrow Cp_2ZrCH_3^+\cdots(\mu_1Cl)MAO\text{-}CH_3Cl^{-*}AlCl_3$ (Site 2)	−85.96 (−85.91)[b]	−95.06 (−95.11)[b]	9.10

[a] Energy difference expressed in kcal/mol.
[b] Energy difference with BSSE correction (expressed in kcal/mol).

Table 6 shows that the formation of ionic species from dichloride zirconocene when the $AlCl_3$ is present is a chemical reaction highly favored from a thermodynamically point of view (Eq. (2)). Conversely, for Eq. (3) the values of ΔE are lower in magnitude by 40 kcal/mol. In spite of the earlier results, the reactions of Eq. (1) involve much higher exothermic processes than Eqs. (2) and (3), which have at least half the magnitude of ΔE for Eq. (1). The column 5 in Table 6 indicates how the $AlCl_3$ benefits the active sites formation. The negative values of ΔE account for the processes of formation of active sites, which are thermodynamically promoted in presence of additive.

The use of BSSE correction [17] according to the standard full counterpoise method is valid to cases where non-significant geometrical changes are present [18,19]. This condition is accomplished only for Eq. (3) (ionic-pair dissociation), but not for the active sites formation from the Cp_2ZrCl_2 and MAO reactives. The corresponding corrected energy values have been reported in Table 6. We observe that they are very small, suggesting that the used basis set is satisfactory for reaction energy calculations.

In order to make a deeper analysis of basis sets dependence, single point calculations have been performed using 6-31G and 6-31G** basis sets for the optimized geometries obtained using 3-21G** basis set. The results are summarized in Table 7. We notice that using the new basis sets the predicted reaction energies decrease in magnitude. The better basis set that includes polarization effects gives values nearly 10% lower than those corresponding to the 3-21G** basis, showing that they are of satisfactory accuracy.

As it was studied by several authors, the Lewis acidity of cocatalyst is evidenced in the alkylation reaction of dichloride metallocene L_2MtX_2 (as it was presented in Section 4.1) and in the X^- anion extraction (X: halogen or alkyl group) from the alkylated neutral metallocene precursor L_2MtRX (L: π-ligand; R: alkyl group) [2d,12a,12b,15b,20]. By this reason, it is convenient to evaluate the Lewis acid power of $AlCl_3$-modified MAO model also in the chloride ion abstraction. For this purpose, the Site 2 is the more appropriated because it is free of steric hindrance effects. The results obtained are compared with those of cocatalyst model without $AlCl_3$ (see Eq. (4)).

$$Cp_2ZrClCH_3 + \text{MAO-}CH_3(\text{or MAO-}CH_3{}^*AlCl_3) \rightarrow \text{Site 2 (or Site 2}^*AlCl_3) \quad (4)$$

The calculated ΔE values show once more that MAO-$CH_3{}^*AlCl_3$ has a higher Lewis acidity than cocatalyst without additive (−103.51 kcal/mol versus −39.49 kcal/mol, respectively). Combining these values with those presented in Section 4.1 for the alkylation dichloride metallocene, it is possible to obtain the balance of total energy for the Site 2 formation (see Table 6, reaction 2). In this way, the chemical effect of $AlCl_3$ on the two sequential reactions that finally form the ionic-pair can be discriminated. The additive favors more the ion chloride abstraction than the alkylation reaction. The abstraction exhibits the highest energetic difference between $AlCl_3$-modified and non-modified active site (increase in ΔE by 2.6 and 1.6 times, respectively).

From the above theoretical results regarding the influence of $AlCl_3$ additive on the chemical equations that take a fundamental role on active sites formation, we observe that the chlorine ion abstraction is more favored than the alkylation reaction, suggesting that in these conditions the reactants will polymerize more rapidly. Moreover, because these active sites become more stable we would expect that the overall formation reaction would also be benefited. The present theoretical results for the Cp_2ZrCl_2/MAO*$AlCl_3$ system are in satisfactory agreement with the experimental data reported for *rac*-$EtInd_2ZrCl_2$/MAO*$AlCl_3$. Indeed, the kinetic curves of propylene polymerization obtained after only a few minutes of reaction in a semi-batch reactor show, with respect to the catalyst without additive, a significant increase of olefin consumption [3b]. Furthermore, this consumption was always higher during the overall polymerization reaction. The theoretical modeling of the kinetic semi-batch reactor data allowed to attain various polymerization properties, such as the propagation constant (kp), the active sites concentration [C^*] or the induction time (t_{ind}) [21]. This study showed an increase of the kpx[C^*] product and a very significant decrease of t_{ind}, i.e. the formation rate of active sites has also been favored. Therefore, it could be concluded that at the presence of $AlCl_3$ the formation of polymerization active sites is favored. This is experimentally expressed as a faster olefin consumption at the beginning of reaction

Table 7
Predicted reaction energies of $Cp_2ZrCH_3{}^+\cdots$MAO-CH_3Cl^- and $Cp_2ZrCH_3{}^+\cdots$ MAO-$CH_3Cl^{-*}AlCl_3$ for both types of sites with 6-31G and 6-31G** basis sets, compared with 3-21G** results

Equation number	Reaction	ΔE with $AlCl_3$ (kcal/mol)		
		3-21G**	6-31G	6-31G**
1	$Cp_2ZrCl_2 + 2$MAO-$CH_3^*AlCl_3 \rightarrow Cp_2ZrCH_3{}^+\cdots(\mu_1O^*)$MAO-$CH_3Cl^{-*}AlCl_3$ (Site 1) + MAO-Cl^*AlCl_3	−202.28	−172.24	−186.90
1	$Cp_2ZrCl_2 + 2$MAO-$CH_3^*AlCl_3 \rightarrow Cp_2ZrCH_3{}^+\cdots(\mu_1Cl)$MAO-$CH_3Cl^{-*}AlCl_3$ (Site 2) + MAO-Cl^*AlCl_3	−211.41	−199.39	−201.75
2	$Cp_2ZrCl_2 + 2$MAO-$CH_3^*AlCl_3 \rightarrow Cp_2ZrCH_3^+ +$ MAO-$CH_3Cl^{-*}AlCl_3 +$ MAO-Cl^*AlCl_3	−125.45	−115.55	−124.22
3	$Cp_2ZrCH_3^+ +$ MAO-$CH_3Cl^{-*}AlCl_3 \rightarrow Cp_2ZrCH_3{}^+\cdots(\mu_1O^*)$MAO-$CH_3Cl^{-*}AlCl_3$ (Site 1)	−76.44	−56.69	−63.68
3	$Cp_2ZrCH_3^+ +$ MAO-$CH_3Cl^{-*}AlCl_3 \rightarrow Cp_2ZrCH_3{}^+\cdots(\mu_1Cl)$MAO-$CH_3Cl^{-*}AlCl_3$ (Site 2)	−85.96	−83.85	−77.53

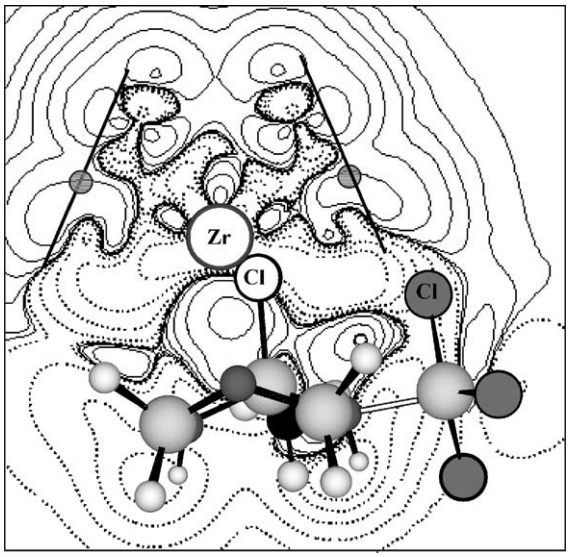

Fig. 5. Charge density difference $\Delta\rho(r)$ for Site 1 ion-pair with $AlCl_3$. Contour plot along the Centr-Zr-Centr plane. Dotted lines correspond to $\Delta\rho < 0$ and solid lines refer to $\Delta\rho > 0$. Dark lines (Cp ligands) and Zr atom were sketched in the picture for better comprehension.

and the continuity of this behavior up to the end of the process.

4.2.4. Density and Laplacian of density analysis

A complementary analysis of electronic density distribution was performed in two selected planes cutting the active sites region. In two cases the planes contain the Zr atom and the centroide point of Cp ligands (Figs. 5 and 7). Additional two planes have were considered: containing the Zr–C_{CH_3}, Zr–O* and Al*–Cl bonds for Site 1 (Fig. 6) and containing the Zr–C_{CH_3}, Zr–Cl, Zr–Al*, O*–Al_{AlCl_3}O*–Al_{AlCl3} and

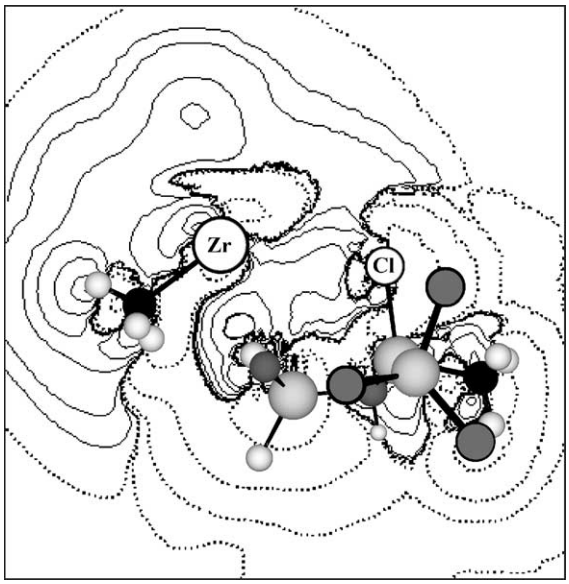

Fig. 6. Charge density difference $\Delta\rho(r)$ for Site 1 ion-pair with $AlCl_3$.

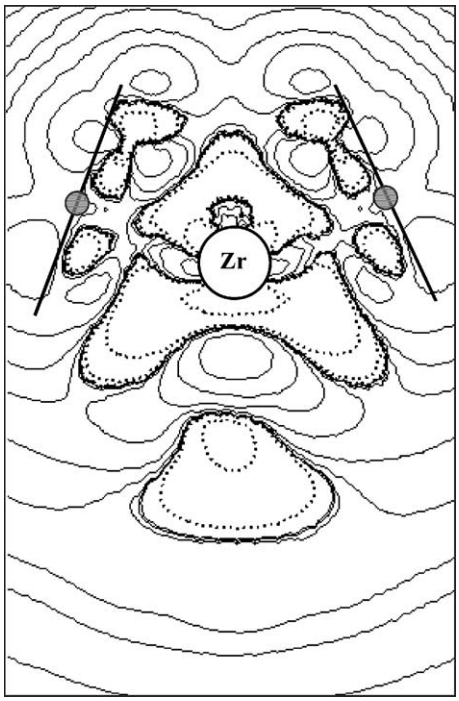

Fig. 7. Charge density difference $\Delta\rho(r)$ for Site 2 ion-pair with $AlCl_3$. Contour plot along the Centr-Zr-Centr plane. Dotted lines correspond to $\Delta\rho < 0$ and solid lines refer to $\Delta\rho > 0$.

$(Al–Cl)_{AlCl_3}$ bonds for Site 2 (Fig. 8). Looking at electronic density distribution in these four planes it is possible to visualize the electron gains for the cation (solid lines), especially in the Cp ligands region, and the electron losses in the $AlCl_3$-modified counterion (dotted lines). These results are in agreement with the modifications of NBO molecular charges of the cation and counterion in active sites with respect to the isolated ions.

Fig. 6 shows the electronic density gain in the region of cation–anion zone interaction which include the Zr–O* and Zr–Cl bonds. The cation-counterion approach produces a negative charge concentration between them. Furthermore, the Zr–C_{CH_3} bond presents negative charge deficiency denoting its weakness.

The Site 2 figures present the same characteristics that were observed for the Site 1. However, the contour plot of the plane containing the centroide-Zr bonds has a completely different distribution, in agreement with the more symmetrical position of $AlCl_3$-modified counterion with respect to the cation (see Fig. 7). Looking at Fig. 8, the electron deficiency in Zr–C_{CH_3} bond and the negative charge accumulation in the interaction region are also evident. Furthermore, the lack of electronic density in Al*–Cl and O*–Al_{AlCl_3} bonds can be visualized. Conversely, the $(Al–Cl)_{AlCl_3}$ bond captures negative charge with respect to the $AlCl_3$-modified counterion. As it was mentioned for Site 1, the electronic density increases in the region surrounding the cation and it decreases in the region where the modified counterion is located.

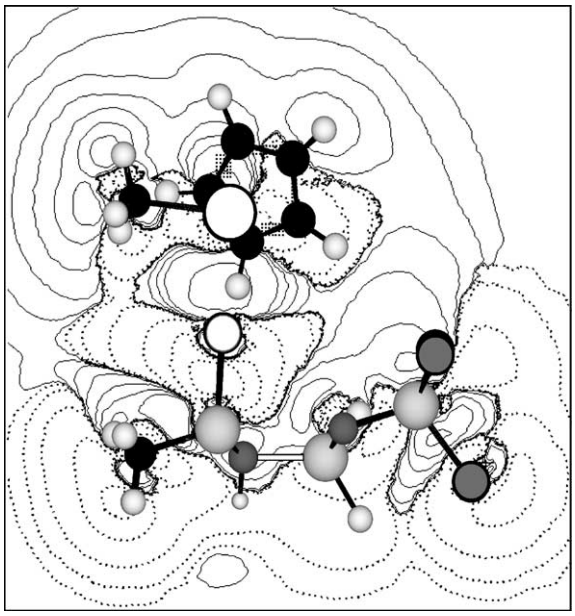

Fig. 8. Charge density difference $\Delta\rho(r)$ for Site 1 ion-pair with $AlCl_3$.

The Laplacian of density $\nabla^2\rho(r)$ for both active sites was calculated. The contour plots of Laplacian for active sites show interesting results to highlight (Figs. 9 and 10). Firstly, the nature of the Zr–C_{CH_3} bond changes with the $AlCl_3$ addition to the counterion for both active sites. While for these sites without additive the Zr–C_{CH_3} bond is covalent [11], with $AlCl_3$ the $\nabla^2\rho(r)$ becomes positive in the Zr–C_{Me} bond zone. This change in sign along the Zr–C_{Me} bond, when the counterion is modified with $AlCl_3$, is an evidence for the more ionic character of the bond. This fact was previously deduced from the NBO atomic charges. Moreover, the Zr–O* bond in Site 1 as well as the Zr–Cl bond in Site 2

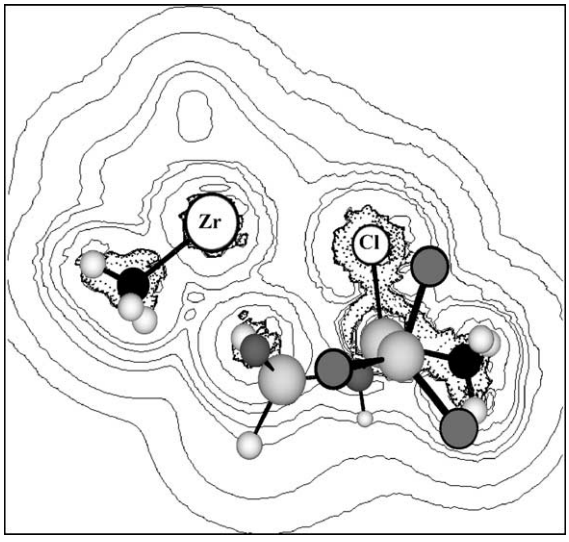

Fig. 9. Laplacian $\nabla^2\rho(r)$ distribution of charge for Site 1. Countour map thorough Zr–C_{CH_3}, Zr–O* bonds (for cation) and Al*–Cl and Al*–C_{CH_3} bond (for MAO-CH_3Cl^{-}*$AlCl_3$ counterion).

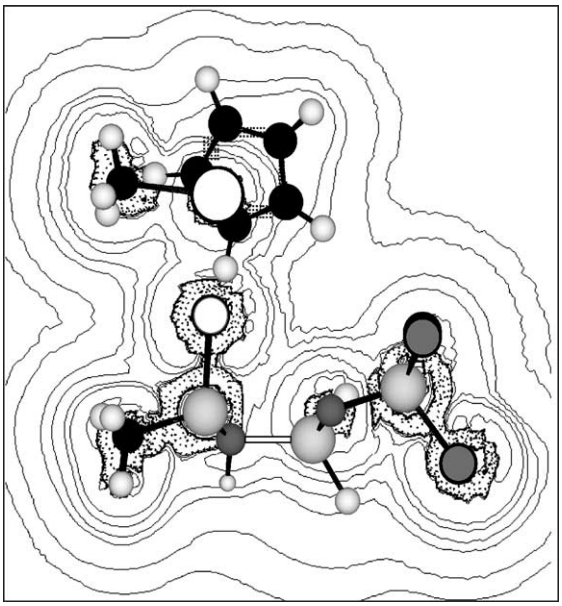

Fig. 10. Laplacian $\nabla^2\rho(r)$ distribution of charge for Site 2. Countour map thorough Zr–C_{CH_3}, Zr–Cl bonds (for cation) and Al*–Cl, Al*–C_{CH_3}, O*–Al_{AlCl_3} $(Al–Cl)_{AlCl_3}$ bonds (for MAO-CH_3Cl^{-}*$AlCl_3$ counterion).

always exhibit ionic character in their cation–anion link. On the other hand, the character of the Al*–Cl bond changes when the active sites are generated with the $AlCl_3$-modified counterion. The negative values of the $\nabla^2\rho(r)$ between Al* and Cl show an important charge electron accumulation in the bond zone, being an evidence of a covalent bond. Similar characteristics were found in the Al–Cl bond of $AlCl_3$. Finally, in Fig. 10 a positive region of $\nabla^2\rho(r)$ can be observed for the O*–Al_{AlCl_3} bond of Site 2. Therefore, the $AlCl_3$ coordination with counterion has an ionic character.

All the exposed results indicate an electronic structure change in the $Cp_2ZrCH_3^{+}\cdots$MAO-CH_3Cl^{-} system with $AlCl_3$ addition. The proposed models predict the Lewis acid modification of MAO when the additive is present. The $AlCl_3$ molecule acts in an indirect way modifying the electrofilicity character of Zr atom. This effect in conjunction with the lability and loss of covalent character of the Zr–C_{CH_3} bond could explain the enhancement of activity in metallocene systems for ethylene and propylene polymerizations. Experimentally, it was observed that the addition of $AlCl_3$ as third component of metallocenic systems favors in 50 and 25% the production of polyethylene and polypropylene, respectively [3].

5. Concluding remarks

From the theoretical results and their discussion presented above we underline the important action of additive on the electronic structure of metallocene systems. The interaction between the different components of the system was studied taking into account recent experimental

results [3]. According to our predictions the previous contact of MAO-CH_3 with the additive enhances the Lewis acidity of the cocatalyst. This conclusion is deduced from the NBO charges analysis. The $AlCl_3$ molecule produces a charge redistribution that weakens the central dative bond $O^* \rightarrow Al^*$ in the cocatalyst and increases its Lewis acidity. This characteristic is confirmed in the energy balances of reactions yielding to the active sites: the alkylation reaction of dichloride catalyst and the chloride abstraction of neutral $Cp_2ZrClCH_3$ precursor.

From the analysis of NBO charges and electron charge mapping, the MAO-$CH_3Cl^{-*}AlCl_3$ counterion releases lower negative charge to the cation than the counterion without $AlCl_3$ additive. The zircocations are more positive, resulting in a more active catalyst. Besides, the stretching of the $Zr–C_{CH_3}$ bond and the lost of its covalent character help to improve the catalytic activity. Indeed, these facts will make more easily to broken this bond and benefit the successive insertions of α-olefins. The olefin insertion into the $Zr–C_{CH_3}$ bond is the most relevant step in the polymerization process via coordination. It is important to underline that the $AlCl_3$ effect on counterion could not be significant on the cation if the active site was not an ionic-pair.

As it was mentioned in Section 1, the predictions obtained from designed models are useful for simulated chemical processes, which complexity avoids a satisfactory characterization. The results showed in this work give possible answers to questions related with the substantial improvement in the performance of catalytic systems when a Lewis acid like $AlCl_3$ is added.

Acknowledgements

We gratefully acknowledge the financial support from the Consejo Nacional de Investigaciones Científicas y Técnicas (CONICET) and the Universidad Nacional del Sur (UNS) for this research.

References

[1] W. Kaminsky, M. Miri, H. Sinn, R. Woldt, Makromol. Chem. Rapid Commun. 4 (1983) 417.
[2] (a) W. Kaminsky, A. Bark, R. Steiger, J. Molec. Catal. 74 (1992) 109;
(b) I. Tritto, S. Li, M.C. Sacchi, G. Zannoni, Macromolecules 26 (1993) 7111;
(c) J.J. Eisch, S.I. Pombrik, G.X. Zheng, Makromol. Chem., Macromol. Symp. 66 (1993) 109;
(d) C.J. Harlan, S.G. Bott, A.R. Barron, J. Am. Chem. Soc. 117 (1995) 6465;
(e) D. Cam, U. Giannini, Makromol. Chem. 193 (1992) 1049;
(f) D. Coevoet, H. Cramail, A. Deffieux, Macromol. Chem. Phys. 199 (1998) 1451;
(g) D. Coevoet, H. Cramail, A. Deffieux, Macromol. Chem. Phys. 199 (1998) 1459;
(h) J. Kim, K.H. Kim, J. Cho, S. Kwak, K.U. Kim, W. Jo, H. Yoon, D. Lim, J. Polym. Sci., A: Polym. Chem. 36 (1998) 1733.
[3] (a) P.G. Belelli, M.L. Ferreira, D.E. Damiani, Macromol. Chem. Phys. 201 (2000) 1458;
(b) P.G. Belelli, M.L. Ferreira, D.E. Damiani, Macromol. Chem. Phys. 201 (2000) 1466.
[4] (a) F. Ruette (Ed.), Quantum Chemistry Approaches to Chemisorption and Heterogeneous Catalysis, Kluwer, Boston, 1992;
(b) S.P. Yuan, J.G. Wang, Y.W. Li, S.Y. Pen, J. Molec. Catal. A: Chem. 178 (2002) 267.
[5] (a) W. Kohn, L. Sham, Phys. Rev. 140 (1965) A1133;
(b) R.G. Parr, W. Yang, Density-Functional Theory of Atoms and Molecules, Oxford University Press, Oxford, 1989;
(c) D.R. Salahub, M.C. Zerner, The challenge of d and f electrons, ACS, Washington, DC, 1989.
[6] M.J. Frisch, G.W. Trucks, H.B. Schlegel, G.E. Scuseria, M.A. Robb, J.R. Cheeseman, V.G. Zakrzewski, J.A. Montgomery Jr., R.E. Stratmann, J.C. Burant, S. Dapprich, J.M. Millam, A.D. Daniels, K.N. Kudin, M.C. Strain, O. Farkas, J. Tomasi, V. Barone, M. Cossi, R. Cammi, B. Mennucci, C. Pomelli, C. Adamo, S. Clifford, J. Ochterski, G.A. Petersson, P.Y. Ayala, Q. Cui, K. Morokuma, D.K. Malick, A.D. Rabuck, K. Raghavachari, J.B. Foresman, J. Cioslowski, J.V. Ortiz, A.G. Baboul, B.B. Stefanov, G. Liu, A. Liashenko, P. Piskorz, I. Komaromi, R. Gomperts, R.L. Martin, D.J. Fox, T. Keith, M.A. Al-Laham, C.Y. Peng, A. Nanayakkara, C. Gonzalez, M. Challacombe, P.M.W. Gill, B. Johnson, W. Chen, M.W. Wong, J.L. Andres, C. Gonzalez, M. Head-Gordon, E.S. Replogle, J.A. Pople, Gaussian'98, Revision A.7, Gaussian, Inc., Pittsburgh, PA, 1998.
[7] (a) R.J. Meier, G.H.J. vanDormemaele, S. Iarloti, F. Buda, J. Am. Chem. Soc. 116 (1994) 7274;
(b) M. Toto, L. Cavallo, P. Corradini, G. Moscardi, L. Resconi, G. Guerra, Macromolecule 31 (1998) 3431;
(c) L. Petitjean, D. Pattou, M.F. Ruiz-López, J. Phys. Chem. B 103 (1999) 27;
(d) P.J. Chirik, J.E. Bercaw, Polym. Preprints 41 (2000) 393;
(e) L. Cavallo, P. Corradini, F. Grisi, P. Longo, G. Guerra, Polym. Preprints 41 (2000) 395.
[8] N.R. Kestner, J.E. Combariza, in: K.B. Lipkowitz, D.B. Boyd (Eds.), Reviews in Computational Chemistry, vol. 13, Wiley, New York, 1999.
[9] (a) E.D. Glendening, A.E. Reed, J.E. Carpenter, F. Weinhold, NBO Version 3.1;
(b) A.E. Reed, L.A. Curtiss, F. Weinhold, Chem. Rev. 88 (1988) 899.
[10] R.S. Mülliken, J. Chem. Phys. 23 (1955) 1833.
[11] P.G. Belelli, M.M. Branda, N. Castellani, J. Molec. Catal. 192 (2002) 9.
[12] (a) M.R. Mason, J.M. Smith, S.G. Bott, A.R. Barron, J. Am. Chem. Soc. 115 (1993) 4971;
(b) A. Barron, Macromol. Symp. 97 (1995) 15;
(c) M. Floor, G.M. Smith, D.B. Malpass, Metallocenes Europe'97, 1997, p. 33;
(d) D.E. Babushkin, N.V. Semikolenova, V.N. Panchenko, A.P. Sobolev, V.A. Zakharov, E.P. Talsi, Macromol. Chem. Phys. 198 (1997) 3855;
(e) H. Sinn, I. Schimmel, M. Ott, N. Von Thienen, A. Harder, W. Hagendorf, B. Heitmann, E. Haupt, in: W. Kaminsky (Ed.), Metalorganic Catalysts for Synthesis and Polymerization, Springer, Berlin, 1999, p. 105;
(f) I.I. Zakharov, V.A. Zakharov, G.M. Zhidomirov, in: W. Kaminsky (Ed.), Metalorganic Catalysts for Synthesis and Polymerization, Springer, Berlin, 1999, p. 129;
(g) M. Ystenes, J.L. Eilertsen, J. Liu, M. Ott, E. Rytter, J.A. Støvneng, J. Polym. Sci.: Part A: Polym. Chem. 38 (2000) 3106.
[13] J. Bliemeister, W. Hagendorf, A. Harder, B. Heitmann, I. Schimmel, E. Shmedt, W. Shnuchel, H. Sinn, L. Tikwe, N. Von Thienen, K. Urlass, H. Winter, O. Zarncke, in: W. Kaminsky (Ed.), Metalorganic

Catalysts for Synthesis and Polymerization, Springer, Berlin, 1999, p. 57.
[14] (a) I. Tritto, S.X. Li, M.C. Sacchi, P. Locatelli, G. Zannoni, Macromolecules 28 (1995) 5358;
(b) R. Fusco, L. Longo, F. Masi, F. Garbassi, Macromolecules 30 (1997) 7673;
(c) M.L. Ferreira, P.G. Belelli, D.E. Damiani, Macromol. Chem. Phys. 202 (2001) 495.
[15] (a) I. Tritto, S.X. Li, M.C. Sacchi, G. Zannoni, Macromolecules 26 (1993) 7111;
(b) I. Tritto, M.C. Sacchi, S.X. Li, Macromol. Rapid Commun. 15 (1994) 217;
(c) I. Tritto, M.C. Sacchi, P. Locatelli, S.X. Li, Macromol. Symp. 97 (1995) 101.
[16] (a) N. Koga, T. Yoshida, K. Morokuma, Ziegler Catalysts, in: G. Fink, R. Mülhaupt, H.H. Brintzinger (Eds.), Springer, Berlin, 1995, p. 275;
(b) V.L. Cruz, A. Muñoz-Escalona, J. Martinez-Salazar, J. Polym. Sci.: Part A: Polym. Chem. 36 (1998) 1157;
(c) T.K. Woo, L. Fan, T. Ziegler, in: G. Fink, R. Mülhaupt, H.H. Brintzinger (Eds.), Ziegler Catalysts, Springer, Berlin, 1995, p. 291.
[17] S.F. Boys, F. Bernardi, Mol. Phys. 19 (1970) 553.
[18] N. Lopez, F. Illas, G. Pacchioni, J. Am. Chem. Soc. 121 (1999) 813.
[19] N. Lopez, F. Illas, G. Pacchioni, J. Phys. Chem. B 103 (1999) 1712.
[20] C.H. Lee, S.J. Lee, J.W. Park, K.H. Kim, B.Y. Lee, J.S. Oh, J. Molec. Catal. A: Chem. 132 (1998) 231.
[21] P.G. Belelli, M.L. Ferreira, M.H. Lacunza, D.E. Damiani, A. Brandolin, Polym. Eng. Sci. 41 (2001) 2082.